Solution of the Unsteady Euler Equations for Fixed and Rotor Wing Configurations

N. L. Sankar,* B.E. Wake,† and S. G. Lekoudis‡
Georgia Institute of Technology, Atlanta, Georgia

A solution procedure is described for the numerical solution of inviscid rotational flow past fixed and rotor wing configurations. This procedure solves the three-dimensional Euler equations in a body-fitted coordinate system and strong conservation form. The derivatives along the spanwise direction are lagged by one time step, while all the other terms are treated in a fully implicit manner. This leads to a semi-implicit scheme that requires two block tridiagonal matrix inversions and one residual evaluation per point at every time step. This procedure also requires the flow variables to be stored at only one time level. A number of fixed wing and rotor wing calculations are presented to demonstrate the efficiency and accuracy of this procedure.

Introduction

In recent years, a number of techniques have evolved for the numerical solution of unsteady compressible flow past fixed and rotor wing configurations. In most cases, these procedures make use of the potential flow approximations to simplify the mathematical formulation and achieve efficient solutions. Borland et al. have developed a small-disturbance potential flow formulation[1] for the unsteady aerodynamic and aeroelastic analysis of flow over modern wing-alone configurations. Sankar et al.[2] recently developed an unsteady full potential formulation for the aerodynamic analysis of arbitrary wing-alone configurations and applied it to a number of practical configurations, including an advanced fighter wing configuration.[3] Other researchers, including Steger and Caradonna[4] and Bridgeman et al.,[5] have also developed unsteady full potential solvers that are capable of handling wing-alone configurations. The development of flow solvers capable of handling rotor wing configurations has benefited from the above and other developments in the fixed wing technology. Caradonna et al.[6] have developed a three-dimensional small-disturbance potential flow solver capable of handling rotor blades both in hover and in forward flight. Arieli and Tauber[7] have recently reported calculations using the ROT22 code, which is a modified version of the highly successful FLO22 code.

While the potential flow solvers of the type described above can and should be used whenever possible, it is desirable to have computational tools that can complement these solvers when the potential flow assumption breaks down. For example, the potential flow formulations just described do not allow for distributed vorticity in the flowfield. In rotor wing and in high angle of attack fighter aircraft applications, a large part of the flowfield in the immediate vicinity of the wing surface is rotational. Also, potential flow solvers tend to overpredict the lift, drag, and pitching moment coefficients whenever the freestream Mach number or angle of attack is very high. Finally, there is no easy way to account for massive separations within the potential flow formulation.

Realizing the need for additional computational tools that can complement potential flow solvers, a number of researchers have developed flow solvers based on the unsteady Euler equations. Jameson and his co-workers[8] have developed a flow solver called FLO-57, which solves the unsteady Euler equations for wing-alone configurations using a four-step Runge-Kutta scheme. Since steady flow solutions were of primary interest in the application, a number of strategies, such as local time steps, enthalpy damping, and multigrid techniques have been built into the solver. Pulliam and his coworkers[9] have also developed Euler solvers capable of handling a variety of two- and three-dimensional configurations.

The choice of Euler equations as the governing equations in these applications arose from the following reasoning. Euler equations admit distributed vorticity fields and capture and convect the vorticity. They also give the correct lift, drag, and moment predictions for high Mach number and high angle of attack applications. Finally, Euler solvers can be easily upgraded into Navier-Stokes solvers capable of handling separated flows, as faster computers with larger core memory become routinely available.

In the present work, the Euler equations were chosen as the governing equations for the reasons just stated. Since rotor wing applications are frequently unsteady by nature, the unsteady Euler equations are solved in this work in a time-accurate manner without resorting to strategies, such as local time steps and enthalpy damping. As the grid spacing varies rapidly over the computational domain, an explicit scheme, such as the one used in Ref. 8, would lead to very small time steps. On the other hand, implicit solvers, such as those described in Ref. 9, lead to larger operation counts and can be difficult to vectorize. After examining a number of strategies, such as locally one-dimensional schemes (LOD), fractional step schemes, etc., a hybrid solution procedure was chosen for solving the equations. This solution procedure has the following advantages:

1) It requires storage of flow variables at only one time step. Solvers such as those described in Refs. 8 and 9 require two or more levels of storage.

2) It requires residual calculations and calculation of stabilizing artificial dissipation terms only once per time step. Also, the costly block tridiagonal matrix inversions required in any implicit time-accurate application need be performed only twice per point per time step.

3) Portions of the present solver such as the residual calculation routines may be vectorized.

A number of applications are presented herein for unsteady three-dimensional calculations for fixed and rotor wing applications. While rotor wing applications are of primary interest in the present work, the fixed wing calculations serve as benchmark calculations because of the large number of numerical and experimental data available for

Presented as Paper 85-0120 at AIAA 23rd Aerospace Sciences Meeting, Reno, NV, Jan. 14-17, 1985; received Jan. 29, 1985; revision received Dec. 18, 1985.

*Associate Professor. Member AIAA.
†Graduate Fellow. Member AIAA.
‡Associate Professor. Member AIAA.

fixed wing geometries. Fixed wing calculations also allow comparisons with existing solvers, such as the FLO-57 code, to be done on a straightforward basis.

Mathematical Formulation

The three-dimensional, unsteady Euler equations may be written in a Cartesian coordinate system as follows:

$$q_t + F_x + G_y + H_z = 0 \tag{1}$$

where

$$F = \begin{Bmatrix} \rho u \\ \rho u^2 + p \\ \rho uv \\ \rho uv \\ u(e+p) \end{Bmatrix} \quad G = \begin{Bmatrix} \rho v \\ \rho uv \\ \rho v^2 + p \\ \rho uw \\ v(e+p) \end{Bmatrix} \quad H = \begin{Bmatrix} \rho w \\ \rho uw \\ \rho vw \\ \rho w^2 + p \\ w(e+p) \end{Bmatrix}$$

Here q is the vector containing the conserved flow properties

$$q = \{\rho, \rho u, \rho v, \rho w, e\} \tag{2}$$

The quantity ρ is the fluid density; u, v, and w are the Cartesian components of fluid velocity; and e is the total energy of the fluid per unit volume.

In order to handle arbitrary wing and rotor shapes undergoing arbitrary motions, the present calculations are performed in a computational space ξ, η, ζ, τ related to the physical space (x, y, z, t) through the following arbitrary one-to-one transformation

$$\begin{aligned} \xi &= (x, y, z, t) \\ \eta &= (x, y, z, t) \\ \zeta &= (x, y, z, t) \\ \tau &= t \end{aligned} \tag{3}$$

In the transformed space (ξ, η, ζ, τ), the Euler equations may be written in the following strong conservation form:

$$\hat{q}_\tau + \hat{F}_\xi + \hat{G}_\eta + \hat{H}_\zeta = 0 \tag{4}$$

where the quantities $\hat{q}$, $\hat{F}$, $\hat{G}$, and $\hat{H}$ are given by

$$\begin{aligned} \hat{q} &= q/J \\ \hat{F} &= (\xi_t q + \xi_x F + \xi_y G + \xi_z H)/J \\ \hat{G} &= (\eta_t q + \eta_x F + \eta_y G + \eta_z H)/J \\ \hat{H} &= (\zeta_t q + \zeta_x F + \zeta_y G + \zeta_z H)/J \end{aligned} \tag{5}$$

where J is the Jacobian of transformation given by

$$\begin{aligned} J = {} & \xi_x(\eta_y\zeta_z - \eta_z\zeta_y) + \xi_y(\eta_z\zeta_x - \eta_x\zeta_z) \\ & + \xi_z(\eta_x\zeta_y - \eta_y\zeta_x) \end{aligned} \tag{6}$$

and ξ_t, η_t, ζ_t account for the motion of the grid through formulas such as

$$\begin{aligned} \xi_t &= -x_\tau\xi_x - y_\tau\xi_y - z_\tau\xi_z \\ \eta_t &= -x_\tau\eta_x - y_\tau\eta_y - z_\tau\eta_z \\ \zeta_t &= -x_\tau\zeta_x - y_\tau\zeta_y - z_\tau\zeta_z \end{aligned} \tag{7}$$

The quantities η_x, η_y, etc., are the metrics of transformation related to the quantities such as x_η by the following relationship:

$$\begin{bmatrix} x_\xi & y_\xi & z_\xi \\ x_\eta & y_\eta & z_\eta \\ x_\zeta & y_\zeta & z_\zeta \end{bmatrix} = \begin{bmatrix} \xi_x & \eta_x & \zeta_x \\ \xi_y & \eta_y & \zeta_y \\ \xi_z & \eta_z & \zeta_z \end{bmatrix}^{-1} \tag{8}$$

While deriving the above form of the governing equations in the transformed plane, use has been made of the geometric conservation law:

$$\left(\frac{1}{J}\right)_\tau + \left(\frac{\xi_t}{J}\right)_\xi + \left(\frac{\eta_t}{J}\right)_\eta + \left(\frac{\zeta_t}{J}\right)_\zeta = 0 \tag{9}$$

which states that the rate at which the volume of a cell changes is dependent on the rate at which its six faces sweep the physical domain. Care must be taken to satisfy this relationship in order to avoid spurious production of mass, momentum, and energy within computational cells. It is also necessary, as pointed out in Ref. 10, that no spurious mass and momentum sources arise simply from the way quantities such as F_ξ are numerically evaluated.

Before Eq. (4) may be solved for flow past fixed and rotor wing configurations, a body-fitted grid must be supplied. It is also necessary to specify a set of physically consistent boundary conditions on all the solid and fluid boundaries surrounding the computational domain. These two issues are considered in the next two sections.

Body-Fitted Coordinate System

A sheared parabolic coordinate system, originally proposed by Jameson,[11] was used in the present work. In this approach, the wing or rotor blade profile is specified at a number of user input span stations. If there is a break in the planform, then the profile must be prescribed at the break. The user input profiles are assembled at the corresponding span stations as a first step in the grid-generation. Then, a set of computational stations are specified on the blade, and beyond the blade (or wing) tip. Eleven equally spaced stations are used on the blade, and 6 stations are placed beyond the blade tip with exponentially growing spanwise spacing. These stations are treated for the grid-generation purposes as an extension of the blade itself, containing infinitesimally thin blade sections. The chord and the leading edge sweep of these off-blade stations are set equal to that of the blade tip.

Linear interpolation is then used along the spanwise direction to generate additional blade profiles at the computational stations. At each of these stations and the stations beyond the tip, a cut is next introduced which leaves the trailing edge along the local camber line and smoothly joins the downstream boundary. Additional points are generated on the blade profile and the cut in order to arrive at a sufficient number of computational nodes at each spanwise station. A cubic polynomial interpolation routine is used for this purpose. In much of the work, 81 computational nodes have been used at each station, 51 of which were directly placed on the profile (26 above, 26 below) with the leading edge being a common node). In rotor blade calculations 161 streamwise nodes were used in the ξ direction, and 23 stations were used along the spanwise direction.

At each span station, a singular point is located just inside the airfoil nose. The profile (x, y) at each spanwise (z) station is unwrapped about this singular point (x_0, y_0) using the following square root transformation:

$$A(x', y') + iS(x', y') = \sqrt{(x - x_0) + i(y - y_0)} \tag{10}$$

Here (x', y') is an intermediate plane. On this plane, a sheared Cartesian coordinate system is next constructed us-

ing a family of lines parallel to the y axis, and a family of lines that are parallel to (i.e., equidistant from) the surface $S(x', y')$. The spacing between this second family of lines is determined by an exponential stretching relationship.

After a sheared Cartesian coordinate system is generated on the (x', y') plane, the nodes on this grid are mapped back onto the physical space (x, y, z) by applying Eq. (10) in reverse. This process is applied at each and every span station, both on and off the blade.

This procedure for generating the grid is extremely fast and may be used for a number of blade and wing shapes, which may contain multiple breaks in the planform. On computer systems with limited memory, it is not necessary to store the three-dimensional grids x and y everywhere. It is sufficient to store the surfaces $S(x', y')$, $A(x', y')$ and the one-dimensional stretching along the y' direction. The coordinates x and y may then be generated on a point by point basis with as few as 4 multiplications per point.

Since the present formulation is written in a general curvilinear coordinate system, other configurations of interest such as blades with winglet-like devices, wing-body configurations, etc., may also be studied, provided a suitable grid-generation scheme is available.

For wing and rotor calculations involving arbitrary geometry motions, the geometry motions and the associated grid motion may be incorporated using additional geometric sequences. For example, for a pitching blade motion, the x-y grid generated at each z station may be rotated about the pitching axis to generate the grid about the twisted blade. The grid velocities are obtained using simple kinematic relationships. Combined pitching and plunging motions may also be similarly handled.

Once an (x, y, z) grid is available, the metrics are evaluated using simple central difference formulas such as

$$x_\xi = (x_{i+1} - x_{i-1})/2$$

$$z_\zeta = (z_{k+1} - z_{k-1})/2 \tag{11}$$

At the boundaries, three-point one-sided differences were used. The other metrics such as X_η etc., were then computed using Eq. (8). The metrics and the coordinates were not stored in order to keep the memory requirements reasonably small. These quantities were recomputed as and when needed.

Boundary Conditions

In the case of both the fixed and rotor wing calculations, the flow was assumed to be undisturbed in the forward (C) part of the sheared parabolic grid. For wing-alone calculations and the rotor in forward flight calculations, this requires the specification of freestream velocities, density, and pressure on this boundary. For a rotor blade in hover, the freestream velocity is set to zero. At the last spanwise station outboard of the wing or blade tip, the flow was also assumed to be undisturbed.

At the downstream part of the farfield boundary, the pressure was prescribed to be the freestream pressure. The normal and two tangential velocities were extrapolated from the interior of the flow using three-point formulas. The density was also similarly extrapolated from the interior.

At the cut that joins the blade trailing edge with the downstream boundary, simple averaging was used from above and below after the interior points had been updated. This leads to some smearing of the entropy layers that arise from the shock waves above and below the blade, but appears to cause no adverse effect. At the span stations outboard of the wing, the flow properties were averaged from above and below, after the interior points were updated. The flow properties at the singular line beyond the wing tip were computed as averages of the flow properties at adjacent points.

Treatment of the Blade Wake

The boundary conditions just described work well for a number of fixed wing calculations and nonlifting rotor wing calculations both in hover and in forward flight. However, when applied to the lifting rotor wing problem, the approach predicts a lift distribution that is substantially larger than that predicted by experiments. This is due to the fact that no account has been made of the strong downwash velocities induced by the tip vortex over the rotor blade.

In Fig. 1, an isolated rotor blade and its associated wake system is shown. This wake produces a large downwash over the entire rotor disk even when the rotor is lightly loaded. In Fig. 2, the rotor disk is shown, and the location of the farfield boundaries of the computational domain are shown. Since the present computational domain covers only a small part of the rotor disk, this helical vortex would enter and leave the outer boundaries of the computational domain at a number of points. The present "no disturbance" boundary conditions do not acknowledge the presence of this helical vortex, although the downstream boundary conditions are such that the helical vortex, when properly introduced at the upstream boundary, will smoothly leave the downstream boundaries. It is the fact that the present boundary conditions do not acknowledge the presence of the helical vortex that leads to the overprediction of the spanwise lift coeffi-

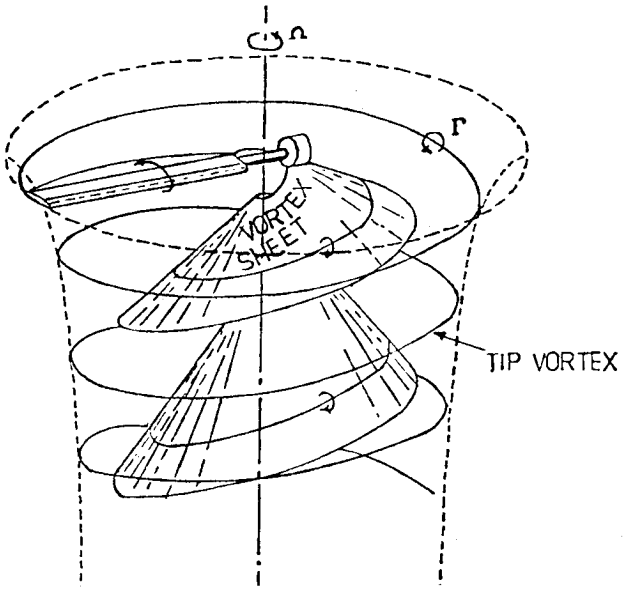

Fig. 1 Schematic diagram of a hovering rotor wake.

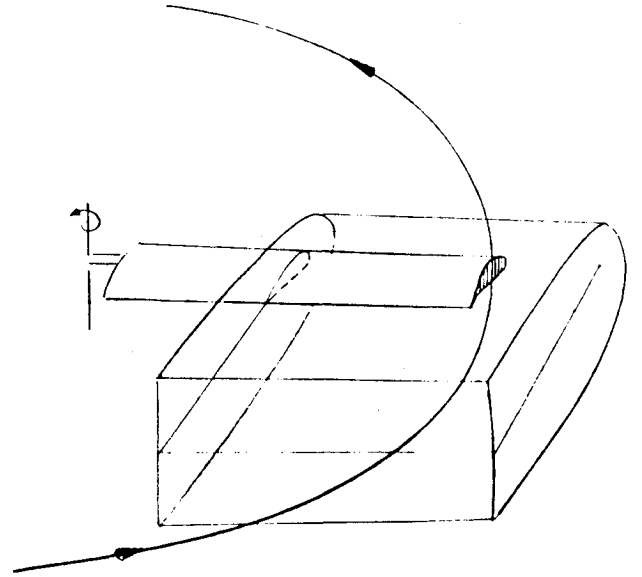

Fig. 2 Schematic diagram of the computational domain.

cients. This undesirable situation can be corrected in a number of ways.

In one possible solution, the computational domain may be enlarged to enclose the entire rotor disk. Then, assuming that the Euler solver produces a tip vortex of correct strength without resorting to viscous mechanisms, this vortex will be captured by the flow and allowed to take the helical form shown in Fig. 1. This solution is the ideal solution for single and multibladed rotor calculations because it does not rely on a wake model. Of course, in order to prevent the artificial viscosity in any numerical scheme from diffusing and distorting the helical vortex, these artificial viscosity terms (to be discussed below) should be modified in the vicinity of the vortex. One such modification to the artificial dissipation terms has been suggested and verified for two-dimensional problems in Refs. 12 and 13.

A second alternative is to expand the flowfield vector q as a combination of $(q-q_w)$ and a q_w field. Here, q_w is a flowfield associated with a helical vortex. If the above decomposition is used in the flux terms appearing in the Euler equations, two groups of terms emerge. One of these groups may be set to zero, based on the argument that the helical vortex and its associated flowfield automatically satisfy the Euler equations. The remainder of the terms lead to a modified set of equations quite similar to the original Euler equations. In fact, this set of equations reproduces the original Euler equations if q_w is set to zero. To illustrate this decomposition, consider the continuity equation written in the Cartesian coordinate system. This equation may be written in terms of $(q-q_w)$ and q_w as follows:

$$\rho_t + (\rho u')_x + (\rho v')_y + (\rho w')_z = -(\rho u_w)_x - (\rho v_w)_y - (\rho w_w)_z \tag{12}$$

where

$$u' = u - u_w, \quad v' = v_w, \quad w' = w - w_w$$

The right-hand side deals with the mass conservation of the vortex flowfield q_w when embedded in a combined flowfield q_w. Based on the argument that the vortex flowfield should automatically satisfy the continuity equation, the right-hand side may be set to zero. Similar decomposition of the momentum and energy equations lead to a set of equations for the unknown vector $(q-q_w)$.

The boundary conditions must be rewritten in terms of the new set of unknowns $(q-q_w)$. The fact that the normal velocity of the fluid is zero at the solid surface can be written as

$$(\vec{q}-\vec{q}_w)\cdot\vec{n} = -\vec{q}_w\cdot\vec{n} \tag{13}$$

This approach assumes that the velocity field associated with an isolated helical vortex q_w is known. It turns out that a velocity distribution that satisfies the right-hand side of Eq. (13) is difficult to find, particularly in compressible flow problems. An approximate velocity field q_w may, however, be found by solving the problem using an incompressible

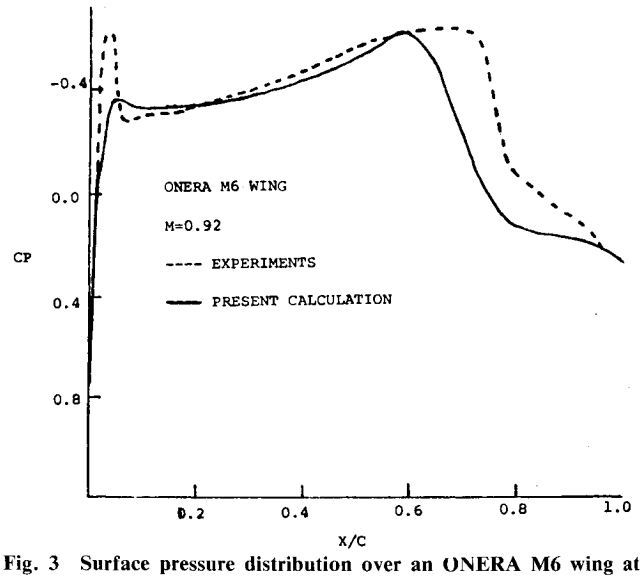

Fig. 3 Surface pressure distribution over an ONERA M6 wing at 65% span (Mach number = 0.923 and angle of attack = 0).

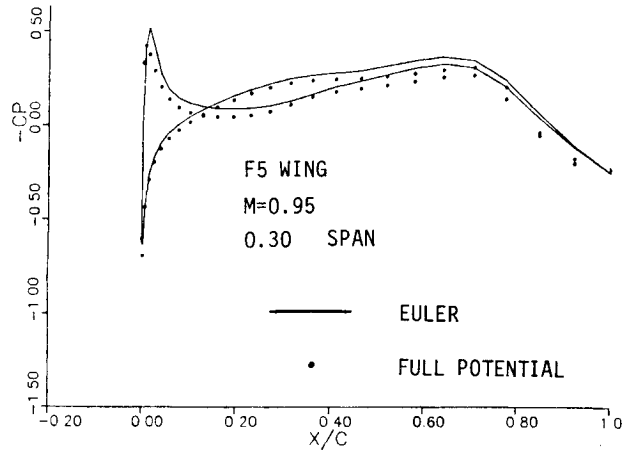

Fig. 4 Surface pressure over an F-5 wing at 30% span (Mach number = 0.95 and angle of attack = 0).

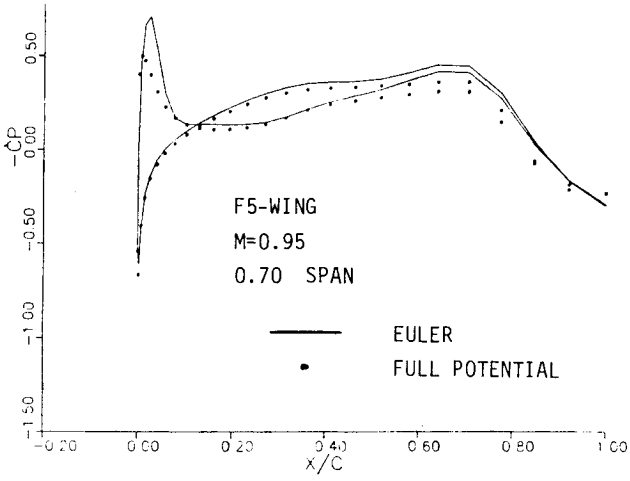

Fig. 5 Surface pressure over an F-5 wing at 70% span (Mach number = 0.95 and angle of attack = 0).

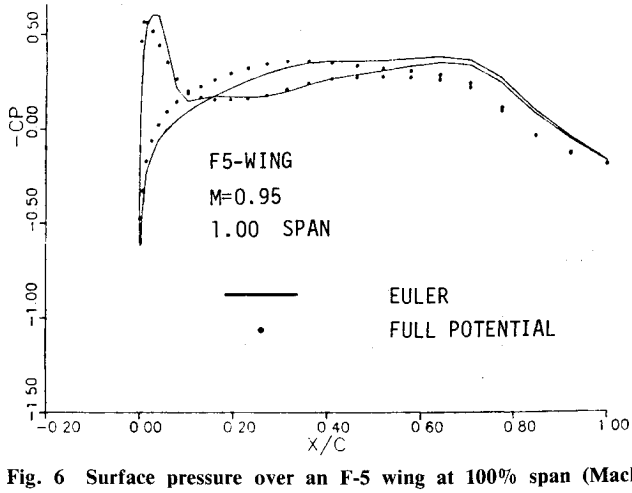

Fig. 6 Surface pressure over an F-5 wing at 100% span (Mach number = 0.95 and angle of attack = 0).

flow approach, such as a lifting line or lifting surface technique. The velocity field associated with the tip vortex can then be found using a Biot-Savart law type of formulation.

Note that with this approach, only a very small portion (the first three η planes around the blade) of the velocity field $(u, v, w)_w$ associated with the blade need be stored. In addition, the majority of the effect on lift is due to w_w, the component normal to the rotor disk. Therefore, the other two components u_w and v_w may be neglected. This assumption should be adequate inboard but is likely to cause large errors in the vicinity of the tip.

In the present work, the second approach discussed with the additional approximations just mentioned was used. The downwash velocities associated with the tip vortex were determined by the application of the Biot-Savart law to a fixed helical vortex with an exponential contraction. The strength of this vortex increased linearly in the vicinity of the tip, but had a fixed constant value everywhere else. Details of this particular tip vortex model are given in Ref. 14.

For the sake of clarity, in what follows, only the formulation based on the combined flowfield q will be discussed. The $q-q_w$ formulation may be obtained from the q formulation in a relatively straightforward manner.

It may be noted that Caradonna et al.[6] have used a prescribed vortex model and its associated downwash field in their small-disturbance potential formulation. To our knowledge, the present work constitutes one of the first attempts to compute lifting rotor flows using the Euler equations with an approximate but consistent treatment of the tip vortex.

Numerical Formulation

The Euler equations are hyperbolic in time. They may be solved by marching in time using any stable, dissipative solution technique. When one is available, steady-state solution may be obtained at asymptotically large time levels following an impulsive start.

In recent years, explicit as well as implicit numerical schemes have been proposed for three-dimensional Euler equations. The MacCormack scheme was one of the earliest explicit schemes to be applied to three-dimensional fluid flow problems. Recently, Jameson[8] has developed a four stage Runge-Kutta scheme for steady and unsteady flows. The explicit schemes in general are limited to very small time steps due to stability limitations and are, therefore, not suitable for unsteady calculations requiring time integrations over large time periods. The explicit schemes also are limited by the amount of "artificial dissipation" that may be added at every time step. In unsteady calculations involving large amplitude impulsive motions, this may be a serious limitation. For these reasons, explicit schemes were not considered in the present study.

Implicit approximate factorization techniques such as the ones used in Ref. 9 allow fairly large time steps to be taken. Although these schemes may be shown to be unconditionally unstable, such instabilities are seldom encountered in practical calculations. However, implicit schemes are computationally expensive on scalar machines because they require three tridiagonal matrix inversions at each time step. The implicit schemes as well as the explicit schemes discussed above require the flow variables to be stored at two or more time levels.

In an attempt to reduce the number of arithmetic operations required at each time level, and to reduce the memory requirements to approximately half of that required by the solvers just described, a hybrid (implicit-explicit) procedure is employed in the present study. A similar procedure has recently been used by Rizk and Chaussee.[15] In the present work, the Euler equations written in the (ξ, η, ζ, τ) domain are discretized in space and time as follows:

$$\frac{\Delta\hat{q}^{n+1}}{\Delta t}+\delta_\xi\hat{F}^{n+1}+\delta_\eta\hat{G}^{n+1}+\delta_\zeta\hat{H}^{n}=0$$

where

$$\Delta\hat{q}^{n+1}=\hat{q}^{n+1}-\hat{q}^{n} \tag{14}$$

Here Δt is the time step by which the solution is advanced. The superscripts n and $n+1$ represent the current time level where the solution is known, and the next time level where the solution is sought. The δ_ξ, δ_η, δ_ζ operators are standard central difference operators. Note that the spanwise derivatives involving H are lagged behind the other two derivatives by one time step. This is in contrast to a fully implicit scheme where all the spatial derivatives are kept at the new $(n+1)$ time level. A von Neumann analysis applied to the model equation

$$q_t+aq_x+bq_y+cq_z=0 \tag{15}$$

and numerical experiments with the present Euler solver indicate that this solver is stable for fairly large time steps, provided the spatial steps along the span direction are larger than the spatial steps along the ξ and η directions.

To avoid odd/even decoupling and prevent high frequency errors from growing and destroying the solution, an explicit fourth order dissipation term is added to the right-hand side of the discretized Eq. (15). This term is of the form:

$$D^n=-\epsilon_E J^{-1}[(\Delta_\xi\Delta_\xi)^2+(\Delta_\eta\Delta_\eta)^2+(\Delta_\zeta\Delta_\zeta)^2]J\hat{q}^n \tag{16}$$

Here ϵ_E is a coefficient which controls the amount of artificial dissipation. For the grid used in most of these calculations, this constant was varied between 2 and 5.

The above artificial dissipation expression is only weakly conservative. Also, in the vicinity of shocks an overshoot occurs when this form is used. Jameson[8] has proposed an artificial dissipation form, which automatically switches to a second order form in the vicinity of shocks. This form has been tested in a two-dimensional version of the present code and has been found to be very useful.[12]

At the innermost span station, Eq. (14) and the artificial dissipation form given in Eq. (16) were used for rotor problems. But the spanwise (ζ) derivatives were dropped at this station, leading to a two-dimensional solution. This solution was allowed to evolve as the interior solution developed.

Equation (14) is highly nonlinear. Therefore, the terms F and G at time levels $(n+1)$ were expanded about their corresponding values at time level n. This gives

$$\hat{F}^{n+1}=\hat{F}^{n}+\left(\frac{\partial\hat{F}}{\partial\hat{q}}\right)^n\Delta\hat{q}^{n+1}+\ldots=\hat{F}^{n}+\hat{A}^n\Delta\hat{q}^{n+1}$$

$$\hat{G}^{n+1}=\hat{G}^{n}+\left(\frac{\partial\hat{G}}{\partial\hat{q}}\right)^n\Delta\hat{q}^{n+1}+\ldots=\hat{F}^{n}+\hat{B}^n\Delta\hat{q}^{n+1} \tag{17}$$

If this expansion is substituted into Eq. (14) and the terms involving $\Delta\hat{q}$ are grouped on the left-hand side, these terms may be approximately factored equation results:

$$\left[I+\frac{\Delta t}{2}\delta_\xi\hat{A}^n-\frac{\epsilon_I}{J}\Delta t(\Delta_\xi\nabla_\xi J)\right]$$

$$\times\left[I+\frac{\Delta t}{2}\delta_\eta\hat{B}^n-\frac{\epsilon_I}{J}\Delta t(\Delta_\eta\nabla_\eta J)\right]\Delta\hat{q}^{n+1}$$

$$=-[\hat{F}_\xi+\hat{G}_\eta+\hat{H}_\zeta+\hat{D}]^n\Delta t \tag{18}$$

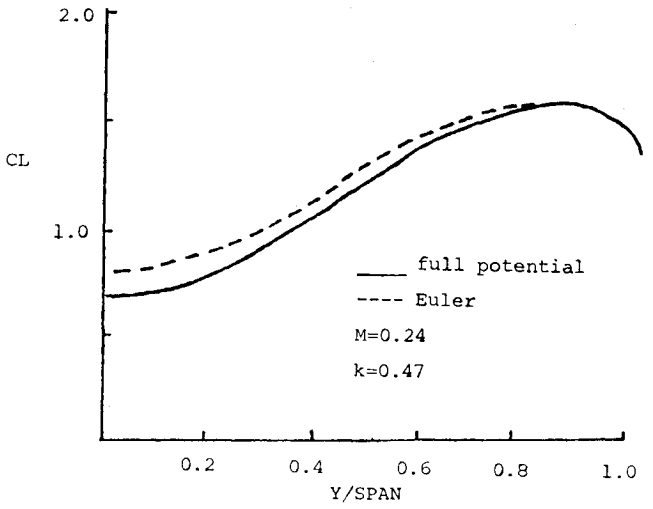

Fig. 7 Lift magnitude variation along the span of a rectangular wing, oscillating in the first bending mode.

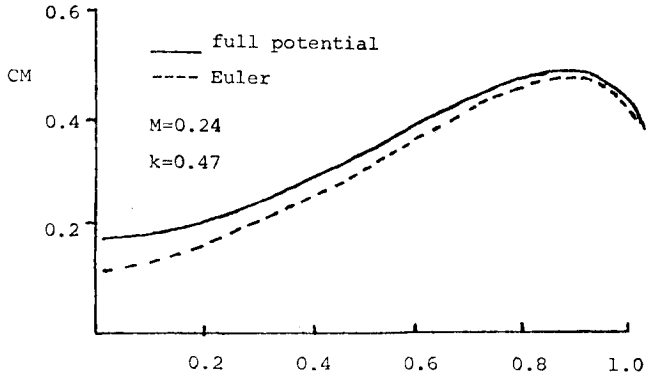

Fig. 8 Pitching moment magnitude variation along the span of a rectangular wing, oscillating in the first bending mode.

Note that the second order terms involving the factor are implicit smoothing factors which must be included in order to allow fairly large values of the explicit dissipation coefficient ϵ_E. In the present work, this coefficient ϵ_I was chosen to be $3\epsilon_E$.

Equation (18) may be solved at each time step using two tridiagonal matrix inversions, one along the η direction and the other along the ζ direction. Note that the solution procedure may be constructed such that the solution vector q need be stored at only one time level. Since residual and dissipation evaluations are performed only once per time step and only two tridiagonal inversions are required per time step, the present algorithm is computationally efficient.

For possible variations on the implicit-explicit algorithms of the type described here, the reader is referred to Ref. 15.

The boundary conditions were explicitly updated in both the fixed and rotor wing problems. Thus the quantity Δq was set equal to zero on all the computational boundaries.

Results and Discussion

A number of fixed and rotor wing calculations have been performed to evaluate the reliability and the accuracy of the solution procedure. Most of the calculations were performed on a CDC CYBER 855 computer system operating under the NOS/VE operating system while some calculations were done on a CRAY X-MP system. Most of the calculations were performed on a rather coarse $81\times17\times17$ grid, while the rotor calculations reported here were performed on a the $161\times23\times16$ grid on the CRAY X-MP computer system.

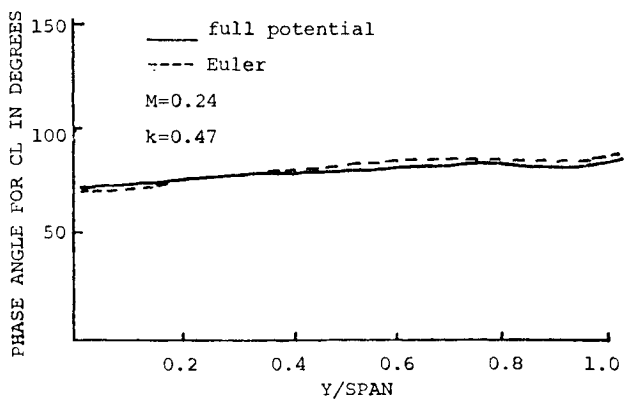

Fig. 9 Lift phase angle variation along the span of a rectangular wing, oscillating in the first bending mode.

The calculations required approximately 1.2 s/time step on the $161\times23\times16$ grid on the CRAY XMP computer system. All the calculations reported here required approximately 400 time steps at a constant time step between .004 and .01 (normalized with respect to tip chord and freestream speed of sound) to converge following an impulsive start. If only a steady-state solution is of interest, part of the above steps may be performed on a coarse grid.

The fixed wing cases were chosen in order to test the stability and the accuracy of the basic algorithm. The wing configurations studied were of low aspect ratio, which leads to a small spanwise grid spacing. Since the present algorithm handled such small step sizes without instability, it is anticipated that large aspect ratio wings and rotor blades will not present any unexpected stability problems.

The first case considered here is an ONERA M6 wing, at zero angle of attack at 0.923 freestream Mach number and zero angle of attack. This wing has been analyzed by a number of researchers. In Fig. 3, the converged surface pressure distribution at the 65% span location, as computed by the present Euler solver, is plotted and compared with some experimental results.[16] The present coarse grid smears the shock pattern somewhat, and the leading edge suction peaks are also underpredicted. Over the rest of the chord the experimental and theoretical data agree fairly well.

An F-5 fighter wing was considered next. This case has also been studied using potential flow methods and experimental techniques in the past. The large leading edge sweep, the small leading edge radius, and the low aspect ratio all make this a difficult configuration to analyze, but an excellent configuration for code validation.

The freestream Mach number was set to 0.95, and the angle of attack was set to zero. In Figs. 4-6 the surface pressure distributions predicted by the present solver are plotted and compared with some full potential flow results.[2] The two methods agree fairly well at a number of inboard stations but differ at the wing tip. The Euler solver tends to predict higher suction levels at the wing tip.

In order to examine the temporal accuracy of the present algorithm and to evaluate its ability to handle moving wing configurations, calculations were carried out for a rectangular wing of (semi-) aspect ratio 2.4, undergoing periodic bending motion, in the first bending mode. The wing sections were made of a NACA 64A010 airfoil shape. In Figs. 7-10, the spanwise lift and moment coefficient variations are plotted in both the magnitude and phase and compared with the predictions of an unsteady full potential flow method. Both the procedures agree very well in their prediction of the phase angles. But the Euler solver tends to underpredict the moment coefficient magnitude, particularly near the wing root.

The calculations performed for fixed wing configurations demonstrate the ability of the present solver to handle ar-

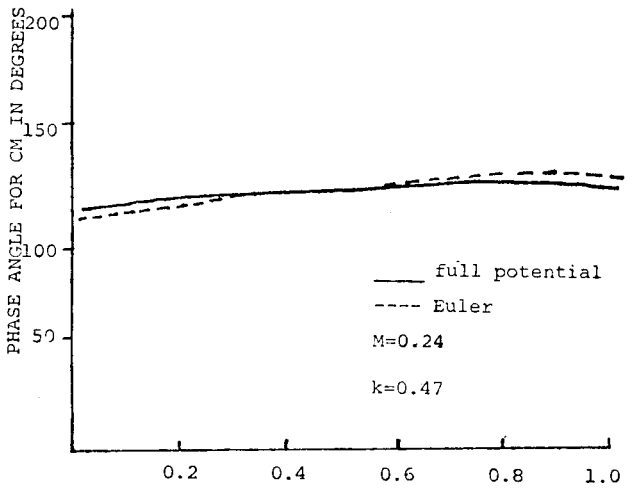

Fig. 10 Moment phase angle variation along the span of a rectangular wing, oscillating in the first bending mode.

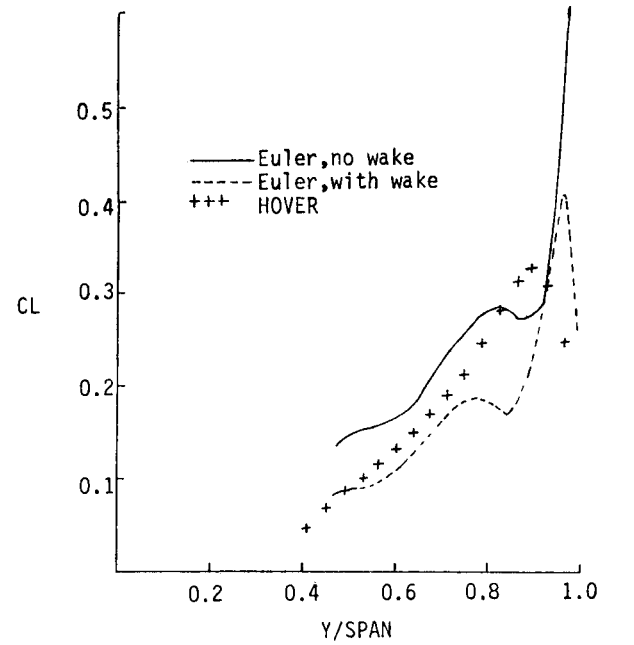

Fig. 11 Spanwise lift variation for an aspect ratio 10 rotor at 6.18 deg angle of attack.

bitrary configurations and arbitrary motions. A number of additional studies must be performed addressing the grid spacing in the vicinity of the wing and wing tip in order to evaluate the small discrepancies between the Euler and the potential flow results just described. Such numerical studies are now in progress.

For rotor calculations, a single-bladed rotor in hover was considered. The blade had an aspect ratio of ten. The first case considered is that of a 6.18 deg angle of attack and tip Mach number of 0.24. The sectional lift coefficients based on tip dynamic pressure are plotted vs span in Fig. 11. These are compared with Euler results without the wake and results from a lifting surface code, HOVER, developed by Summa and his co-workers.[17] The Euler results without the wake are, as expected, larger than that with the wake. The results obtained in the present study using the empirical wake model discussed earlier agree well with the lifting surface method predictions up to 75% of the span but begin to deviate beyond the 75% span. An examination of the surface pressure distributions in the vicinity of the blade tip showed pressure crossover at the blade trailing edge. It appears that finer grid near the blade trailing edge or a new topography, such as an O-grid system, may be needed to improve the trailing edge pressure closure and the lift distribution.

Conclusions

A solution procedure has been developed for the numerical solution of the three-dimensional Euler equations and applied to steady and unsteady, fixed and rotor wing calculations with encouraging results. Additional studies on denser grids are needed to improve the accuracy of this procedure.

Acknowledgments

This work was supported by the U.S. Army Research Office under the Center of Excellence for Rotary Wing Aircraft Technology program.

References

[1]Borland, C., Rizzetta, D., and Yoshihara, H., "Numerical Solution of Three-Dimensional Unsteady Transonic Flow Over Swept Wings," AIAA Paper 80-1369, 1980.

[2]Sankar, N.L., Malone, J.B., and Tassa, Y., "An Implicit Conservative Algorithm for Steady and Unsteady Three-Dimensional Potential Flows," AIAA Paper 81-1016, 1981.

[3]Malone, J.B., Sankar, N.L., and Sotomayer, W.A., "Unsteady Aerodynamic Modeling of a Fighter Wing in Transonic Flow," AIAA Paper 84-1566, 1984.

[4]Steger, J.L. and Caradonna, F.X., "A Conservative Implicit Finite Difference Algorithm for the Unsteady Transonic Potential Equation," AIAA Paper 80-1368, 1980.

[5]Bridgeman, J.O., Steger, J.L., and Caradonna, F.X., "A Conservative Finite Difference Algorithm for the Unsteady Transonic Potential Equation in Generalized Coordinates," AIAA Paper 82-1388, 1982.

[6]Caradonna, F.X., Tung, C., and Desopper, A., "Finite Difference Modeling of Rotor Flows Including Wake Effects," *Journal of the American Helicopter Society*, April 1984, pp. 26-33.

[7]Arieli, R. and Tauber, M.E., "Computation of Subsonic and Transonic Flow about Lifting Rotor Blades," AIAA Paper 79-1667, 1979.

[8]Jameson, A. and Baker, T.J., "Solution of the Euler Equations for Complex Configurations," AIAA Paper 83-1919, 1983.

[9]Pulliam, T. H., "Euler and Thin Layer Navier-Stokes Codes: ARC2D, ARC3D," Notes for Computational Fluid Dynamics Users Workshop, The University of Tennessee Space Institute, March 12-16, 1984.

[10]Pulliam, T. H. and Steger, J. L., "Implicit Finite Difference Simulation of Three-Dimensional Compressible Flow," *AIAA Journal*, Vol. 18, 1980, p. 159.

[11]Jameson, A., "Iterative Solution of Transonic Flows Over Airfoils and Wings Including Flows at Mach 1," *Communications in Pure and Applied Mathematics*, Vol. 27, 1974, pp. 283-309.

[12]Sankar, N.L. and Tang, W., "Numerical Solution of Unsteady Viscous Flow Past Rotor Sections," AIAA Paper 85-0129, 1985.

[13]Srinivasan, G.R., McCroskey, W.J., and Kutler, P., "Numerical Solution of the Interaction of a Vortex with a Stationary Airfoil in Transonic Flow," AIAA Paper 84-0254, 1984.

[14]Shenoy, K.R. and Gray, R.B., "Iterative Lifting Surface Method for Thick Bladed Hovering Helicopter Rotors," *Journal of Aircraft*, Vol. 18, June 1981, pp. 417-424.

[15]Rizk, Y.M. and Chaussee, D.S., "Three-Dimensional Viscous Flow Computations Using a Directionally Implicit-Explicit Procedure, AIAA Paper 83-1910, 1983.

[16]Monnerie, B. and Charpin, F., "Essais de buffeting d'une aile en fleche transsonique," 10e Colloque d'Aérodynamique Appliquée, Lille, France, 1973.

[17]Summa, J.M. and Clark, D.R., "A Lifting Surface Method for Hover/Climb Loads," 35th Annual Forum of the American Helicopter Society, Preprint 79-1, May 1979.